BOLETÍN GEOLÓGICO Y MINERO
2024, VOL. 135 (1), 43-57
ISSN-L: 0366-0176
http://dx.doi.org/10.21701/bolgeomin/135.1/003

Boletín Geológico y Minero

RESEARCH ARTICLE

Evidences for a Rotational Variscan Deformation from Distorted Brachiopods (Meseta, Morocco)

Evidencia de una deformación rotacional varisca a partir de braquiópodos distorsionados (Meseta, Marruecos)

Kawtar Nassri[1]*, Abdessamad El Adraoui[1]

[1]Department of Geology, Faculty of Sciences, University Mohammed V, Rabat, Morocco

Corresponding author: kawtar_nassri@um5.ac.ma (Kawtar Nassri)

Key points:

The rarity of deformed objects in the Meseta NW did not allow to define precisely before this work the characteristics of the Variscan deformation.

The discovery of deformed brachiopods in the contact Cherrat- Sidi Bettache basin allowed to quantify this deformation performing a strain analysis.

The parameters obtained indicate a homogenous non-coaxial simple shear strain during EW Variscan shortening.

ABSTRACT

In 2021-2022, the construction work of the coastal road R322, connecting the Kasbah of Oudayas (Rabat) with the seaside resort of Bouznika, has made it possible to observe schists with brachiopods (Spirifer sp.) of the Upper Visean in the Val d'Or beach, 12 km at the SW of Rabat. The structural analysis of the collected samples shows deformed fossils on the XY plane of the slaty cleavage (S_1), affected by D_2 recumbent, west-vergent folds and an associated N-S trending crenulation cleavage (S_2). The fossils of Spirifer sp. are triangular in shape, recalling a butterfly. The fossils show a bilateral symmetry in their undeformed state, with two perpendicular directions forming a T (sinus or symmetrical line and hinge). After deformation, these lines intersect with an acute/obtuse angle indicating the distortion of fossils. Measurements of the shear angles lead us to reconstruct the Mohr circle referred to strained conditions and obtain the shape and orientation of the finite deformation ellipse. This method makes it possible to find the axial ratio of the finite strain ellipse from Mohr circles. Our results are compared with those obtained by Wellman's method and Breddin abacus. A structural model is proposed to explain the studied ductile deformation, which we suggest it is related to dextral, N-S trending shear zones.

Keywords: Strain Analysis; Ductile Simple Shear; Upper Visean; Sidi Bettache Basin; Val d'Or

Article History:
Received: 12/04/2023
Accepted: 10/11/2023

Puntos clave:

La escasez de objetos deformados en el NO de la Meseta marroquí no permitía cuantificar la deformación varisca.

El descubrimiento de braquiópodos distorsionados (Viseense sup) en el contacto Cherrat-Sidi Bettache ha permitido cuantificar esta deformación.

Los parámetros obtenidos indican deformación rotacional por cizalla simple dúctil durante el acortamiento E-O varisco.

RESUMEN

En 2021-2022, las obras de construcción de la carretera costera R322, que conecta la Kasbah de Oudayas (Rabat) con la localidad costera de Bouznika, han hecho posible estudiar esquistos con braquiópodos (Spirifer sp.) del Viseense sup. en la playa de Val d'Or, 12 km al suroeste de Rabat. El análisis estructural de las muestras recogidas indica una deformación de los fósiles en el plano XY del clivaje pizarroso (S_1), afectados por pliegues recumbentes de vergencia oeste y por una foliación de crenulación (S_2) asociada a los pliegues. Los fósiles de Spirifer sp. son triangulares, con forma de mariposa, y tienen el interés de mostrar simetría bilateral en el estado no deformado, con dos direcciones perpendiculares en T (seno o línea de simetría y charnela). Después de la deformación, estos ejes se cruzan con un ángulo agudo / obtuso que indica una deformación angular. Las medidas de los ángulos de cizalla nos llevan a reconstruir el círculo de Mohr para ángulos en el estado deformado, con objeto de obtener la forma de la elipse de deformación finita y determinar los mecanismos responsables de la distorsión utilizando el diagrama de forma de las elipses. Este método permite determinar la relación axial de la elipse de la deformación finita mediante los círculos de Mohr. Los resultados se comparan con los obtenidos por el método de Wellman y el ábaco de Breddin. Finalmente, se propone un modelo estructural que explica las deformaciones dúctiles observadas como desarrolladas dentro zonas de cizalla dextras de dirección N-S.

Palabras clave: Análisis de la deformación; Cizalla simple dúctil; Viseense superior; Cuenca de Sidi Bettache; Val d'Or.

Historial del artículo:
Recibido: 12/04/2023
Aceptado: 10/11/2023

1. Introduction

The main objective of this work is to highlight, for the first time, the Variscan deformation characteristics of a set of distorted brachiopod fossils recently discovered in the area of "Val d'Or", on the Atlantic coast of the Moroccan Meseta (X : 33,906231,Y : -6,986226). The strain analysis performed in this work provides some finite deformation parameters: elongations, quadratic elongations, and angular strain parameters, which, through the use of the Mohr construction, has yielded the axial ratio and orientation of the finite strain.

2. Geological Setting: West Mesetian Variscan Evolution

The western Meseta of Morocco is mainly subdivided into four structural domains (Piqué, 1994) representing the roots of the Variscan belt. The major deformation events are Namurian-Westphalian in age (Michard, 1976), followed by mostly brittle deformations during the Permian (Ait Brahim and Tahiri, 1996). From west to east we distinguish (figs. 1-A and B):

Coastal Block (MC): located in the westernmost part of the Meseta, this domain is stable, scarcely deformed (Michard, 1976), and composed by continental platform rocks of the Early Paleozoic, namely middle Cambrian quartzites, schists and Ordovician shales. Near the shear zones affecting the region, those rocks are widely folded and show a slaty cleavage (El Attari, 2001). In the oued Rhebar, between Bouznika and Mohamedia, the middle Cambrian schists show a calc-alkaline volcanic complex generated during the Mesetian rift event, with orogenic signatures (El Hadi, 2006).

Benslimane Basin (BBS): defined by Lecointre (1926) and mapped by Destombes and Jeanette (1966) as a NS sheared and compressed furrow, located at the East of the Coastal Block and separated from it by the West Meseta shear zone (WMSZ; figs. 1-A and B). This basin is formed by upper Famennian to upper Visean series that were affected by ductile, semi-brittle and brittle polyphasic deformation under a clockwise rotating principal stress σ_1 (Nassri and El Adraoui, 2022).

Cherrat Ridge (RCH): a N-S Devonian horst, it is mainly constituted by Silurian and Devonian platform carbonates. They were up-righted and sheared (Chalouan, 1977) by a first Variscan deformation phase, D_1, giving place to folds (trending N160ºE) and a fracture cleavage. A second Variscan phase, D_2, originated folds (trending N045ºE), kinks and a crenulation cleavage. Towards the Atlantic Ocean, at Skhirate, Cherrat Ridge is offset towards the East by the E-W to NE-SW dextral strike-slip fault array of Skhirate.

Sidi Bettache Basin (BSB): Defined by Piqué (1979), this basin is filled with thick series of Famennian-Tournaisian and upper Visean ages and subdivided into (Lakhloufi *et al*., 2002, 2008):

- Sidi Bettache Basin s. s. (BSB): individualized during the upper Famennian.
- Brachwa-Maaziz Basin (BBM) filled with upper Visean deposits.

According to the authors cited before, the Sidi Bettache basin was formed first by Famennian NE-SW extension and later by upper Visean transpression (σ_1 : NE-SW). This basin, which northwestern part is studied here, was strongly folded and metamorphosed mainly during the Namurian-Westphalian, and strongly sheared during later Permian phases.

3. Structural outline of the Northwestern Sidi Bettache Basin

We studied here the coastal band of the Sidi Bettache basin, which extends into the central Meseta (figs. 1-A and B). It is formed by Famennian-Tournaisian detrital series covered by thick Upper Visean rocks, including claystones, recifal limestones, coastal sandstones, detrital quartzites, siltstones, mudstones and shales. Close to our sampling point in Val d'Or beach, some of these Visean series crop out in the Sable d'Or beach, showing mainly two phases of deformation:

- D_1 folds trending N170ºE, with vertical or steep, west-dipping axial planes. Folds are accompanied by a slaty cleavage (S_1) often parallel to their axial planes.
- D_2 folds trending N-S, but accompanied by a penetrative crenulation cleavage striking N120ºE to N-S (Fig. 1-C). The localized variation of the directions of S_2 can be interpreted as the result of rotational deformation (possibly dextral transpression). The folds generated by E-W shortening are then sheared by N120ºE dextral strike-slip faults and N160º-N168ºE sinistral strike-slip faults, indicating a late NW-SE compression.

The samples of brachiopods studied in this paper show exclusively ductile deformation associated with D_2.

4. Methodology

In this work we intend to determine the shape and orientation of the finite strain ellipse from deformed fossils (brachiopods) that presented bilateral symmetry before deformation. Finite deformation can be separated into different components: translation, rigid rotation, distortion, and volume or area change. The distortion and the change in volume or area constitute the strain (e.g., Fossen, 2010). In two dimensions, strain can be described by several dimensionless quantities. To measure changes in the length of lines, parameters such as linear extension ($e = (l_1-l_0)/l_0$), elongation ($\lambda = l_1/l_0 = 1 + e$), quadratic elongation ($\Lambda = \lambda^2$), or logarithmic or natural deformation ($\varepsilon = \ln \lambda$) can be used. In all cases, l_1 and l_0 indicate the final and initial length of the line, respectively. On the other side, the shear angle (ψ) measures the change in the angle between two initially perpendicular lines. In this work, ψ is considered positive in case of a clockwise rotation and negative otherwise. Finally, the shear strain parameter, γ, is defined as $\gamma = \tan \psi$. Two-dimensional finite strain is best represented by the strain ellipse, which is the figure obtained by homogeneous strain of an initial circumference of unit radius. Accordingly, the half-length of the principal axes of the finite strain ellipse are $\lambda_G > \lambda_P$. A useful way to represent the shape of the finite strain ellipse and its dimensions with respect to the initial, circumference is the Cartesian diagram λ_G vs. λ_P (Fig. 2) (e.g., Ramsay, 1967).

4.1. Mohr circle of deformation

Each line of the ellipse (Fig. 3) forming an angle θ' in the deformed state with the main axis λ_G is characterized by a reciprocal quadratic elongation: $\Lambda' = \Lambda'_G \cos^2\theta' + \Lambda'_P \sin^2\theta'$.

The corresponding shear is defined as: $\gamma' = (\Lambda'_P - \Lambda'_G) \sin \theta'. \cos\theta'$. Equations Λ' and γ' are a way of expressing the equations of a circle. The reciprocal quadratic elongations Λ', Λ'_P and Λ'_G are obtained by operating the inverse of the quadratic extensions: $\Lambda' = 1/\Lambda$ and

$\gamma' = \gamma/ \Lambda$, $\Lambda'_P = 1/ \Lambda_P$ and $\Lambda'_G = 1/ \Lambda_G$.

In order to determine the deformation ellipse, the previous equations are reformulated as (Ramsay, 1967, 1970; Viallon, 1991):

$\Lambda' = ½. (\Lambda'_P + \Lambda'_G) - ½ . (\Lambda'_P - \Lambda'_G) \cos 2\theta'$ and $\gamma' = ½. (\Lambda'_P - \Lambda'_G) \sin 2\theta'$.

The analysis of the deformation becomes possible by the construction of the Mohr circle, the horizontal axis corresponds to the reciprocal quadratic elongation Λ' and the axis of the coordinates represents the shears γ' (Fig. 3).

4.2. Determination of the deformation ellipse

The determination of the main axis of the ellipse by strain analysis is only possible if the viscosity of the matrix is close to that of deformed objects (Brun and Choukroune in Nicolas, 1984; Michard, 1977, etc.). This condition is verified in our case, since the matrix (organic clay mud) and the material filling by moulding the shells of the Brachiopods Sprifer sp. are identical. We have used brachiopods as deformed objects for the measurement of angular shear deformation (Fig. 4). It should be noted that the Mohr diagram is not to scale.

The interest of the brachiopods, Spirifer sp. in particular, is the presence of two perpendicular lines in the undeformed state: hinge line and sinus symmetry line. After distortion of the fossils, though differently oriented, the shear angle ψ is measured as the angle deviating of the median sinus line relative to its originally perpendicular hinge axis. Plotting in the Mohr space the individual values of ψi of the different individuals makes it possible to find the ratio Λ_G/Λ_P and the shape and orientation of the deformation ellipse (figs. 3 and 4).

We have computed the angular deformation parameters on 14 selected brachiopod fossils distributed on five rock samples taken on an anticline structure (Fig. 1-C), a folded lumachellic layer interbeded in clay-mudstone strata affected by recumbent, west-vergent crenulation microfolds. Samples 1, 2, 3 are taken from the low-dipping limb (S_{0-1} in average N173, 25 E and S_2: N003,90). Sample 4 is taken in the steeply-dipping limb (S_{0-1}: N002, 80W and S_2: N174, 70 E), while sample 5 is taken at the inner part of the hinge of the anticline (S_{0-1}: N005, 85W and S_2: N002,78 E) (figs. 1-C and 5).

Figure 5 shows five horizontal sections taken parallel to layers and slaty cleavage S_{0-1} (D_1). Also, crenulation cleavage (lineation Lc, and S_2) generated during phase D_2 is indicated on each section. The photographs are taken with the north always oriented to the top. In each sample, two or

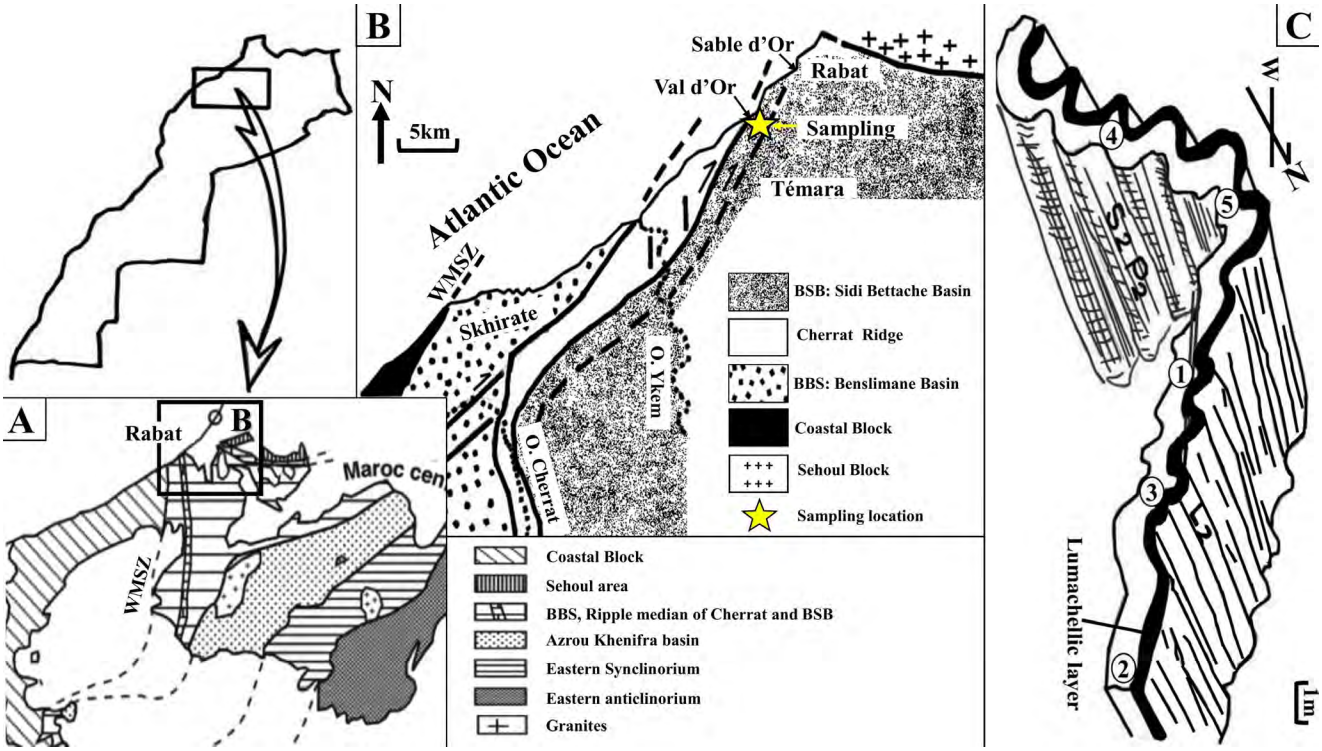

Figure 1. A- Main structural domains of the western Meseta. BBS: Benslimane basin, BSB: Sidi Bettache basin (Piqué *et al.*, 2006); B-Geological sketch map of the northern part of Sidi Bettache basin; C-Studied fold S2P2 and location of samples on the structure.

Figura 1. A- Principales dominios estructurales de la Meseta occidental. BBS: cuenca de Benslimane, BSB: cuenca de Sidi Bettache (Piqué *et al.*, 2006); B- Mapa geológico de la parte norte de la cuenca de Sidi Bettache; C- pliegues S2P2 estudiados y ubicación de las muestras en la estructura.

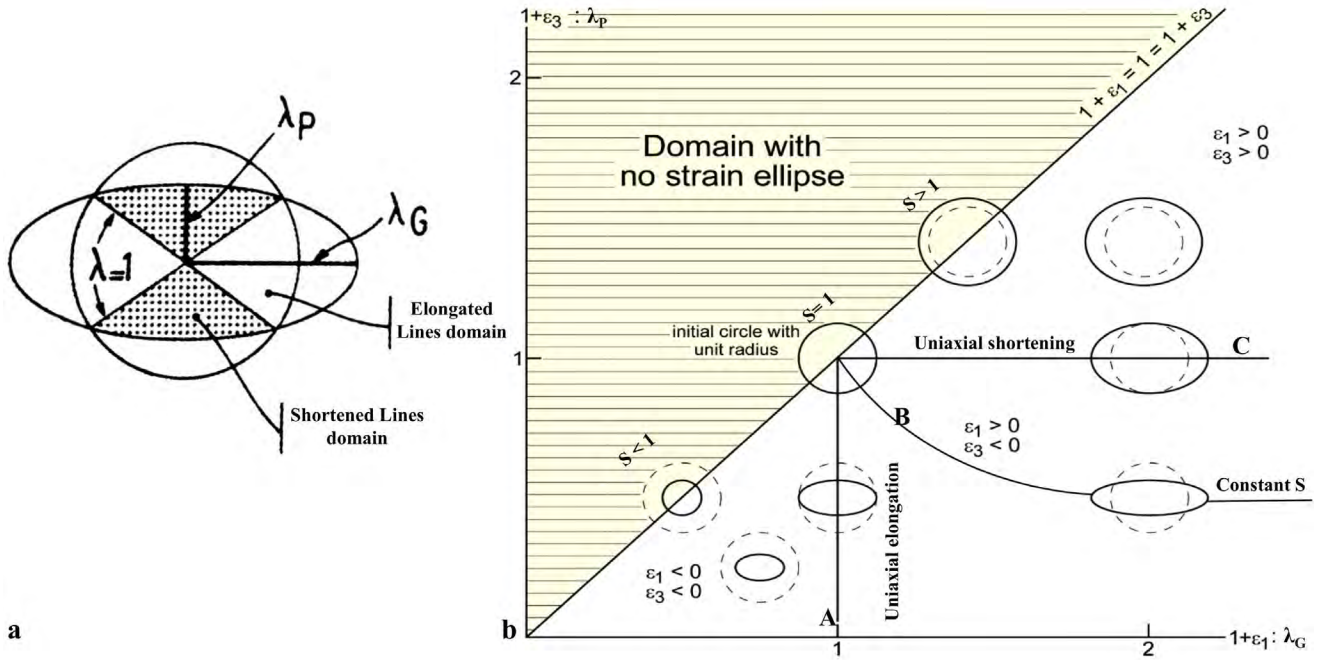

Figure 2. a- Fields of line shortening/elongation from infinitesimal to finite strain in two dimensions (Nicolas, 1984). b-Graphical representation of strain ellipses. https://www.files.ethz.ch/structuralgeology/jpb/files/english/12finitestrain.pdf

Figura 2. a-Campos de acortamiento y estiramiento de líneas para la deformación finita en dos dimensiones (Nicolas, 1984). b-Representación gráfica de elipses de deformación. https://www.files.ethz.ch/structuralgeology/jpb/files/english/12finitestrain.pdf

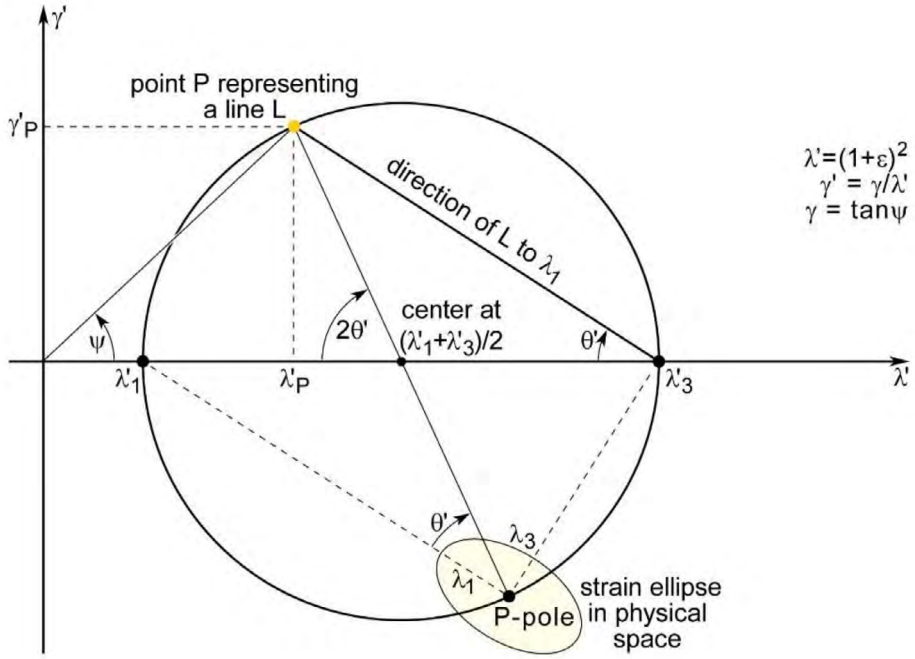

Figure 3. Two-dimensonal Mohr construction for a state of finite strain. https://www.files.ethz.ch/structuralgeology/jpb/files/english/12finitestrain.pdf.

Figura 3. Construcción bidimensional de Mohr para un estado de deformación finita. https://www.files.ethz.ch/structuralgeology/jpb/files/english/12finitestrain.pdf.

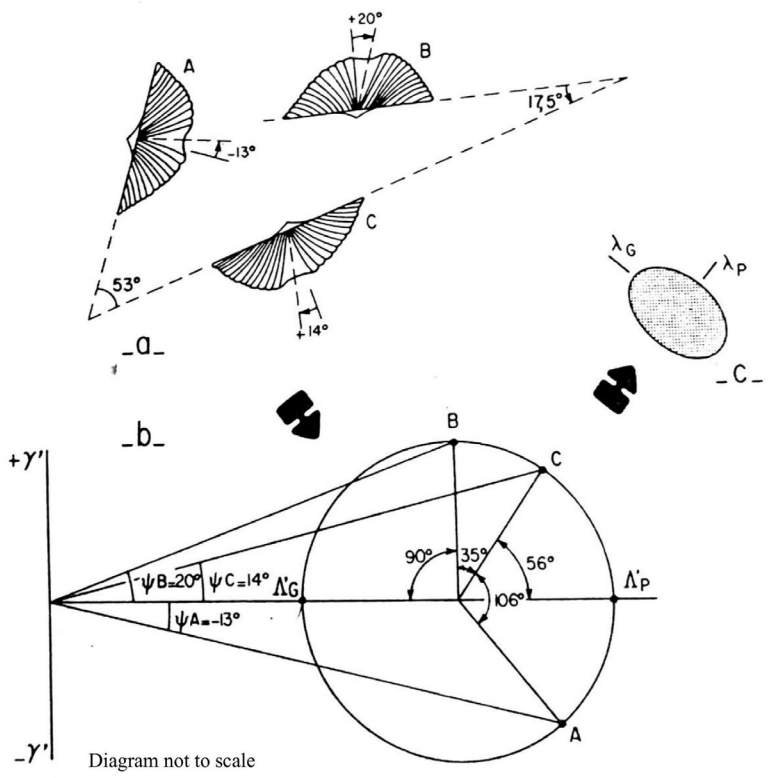

Figure 4. Determination of deformation ellipse from three shear measurements. a:-Deformed brachiopods. b-Mohr construction. c-Corresponding deformation ellipse (Brun and Choukroune in Nicolas, 1984).

Figura 4. Determinación de la elipse de deformación a partir de tres medidas de deformación angular. a-Braquiópodos deformados. b-Construcción del círculo de Mohr. c-Elipse de deformación correspondiente (Brun y Choukroune en Nicolas, 1984).

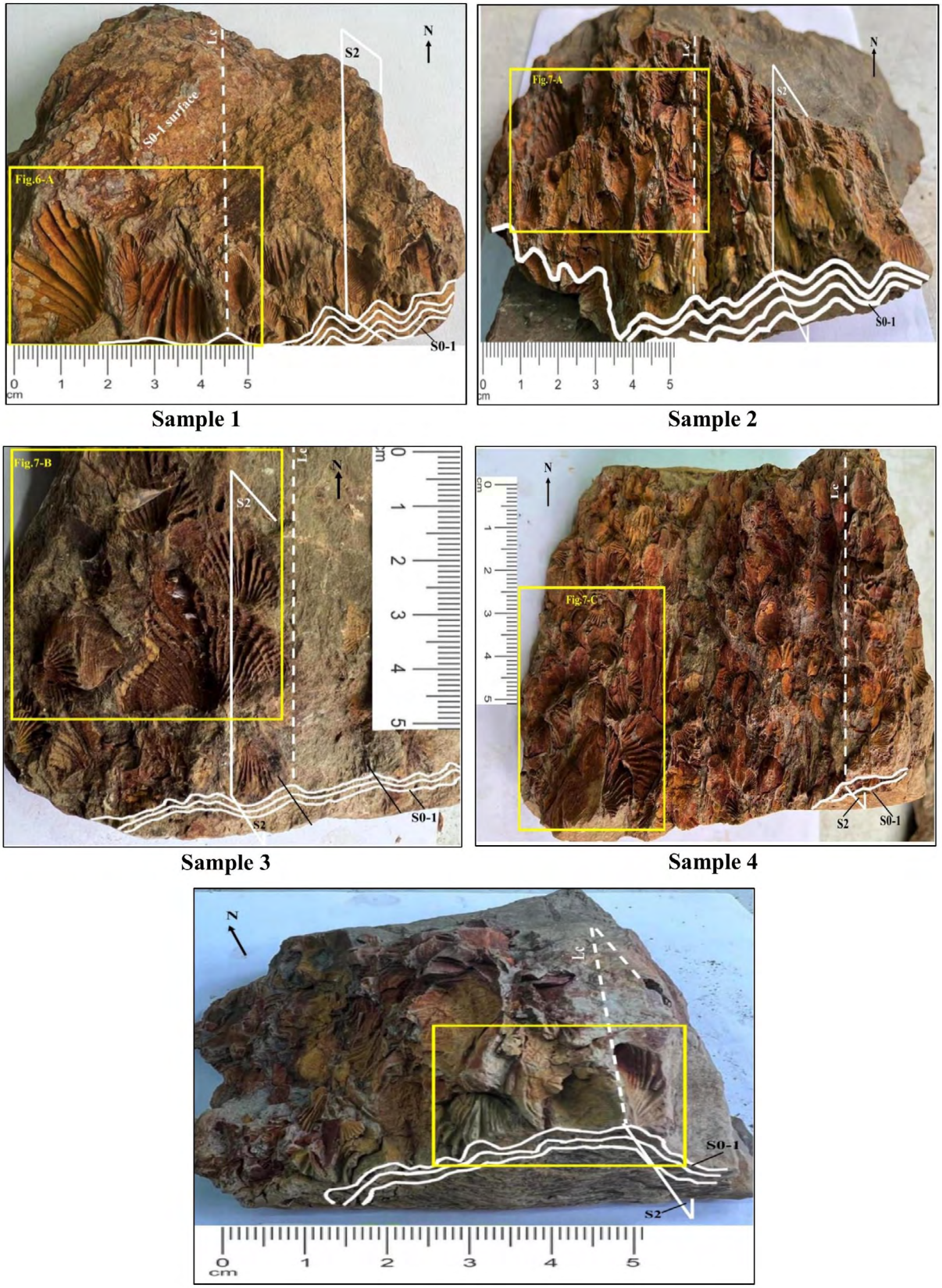

Figure 5. Photographs of the five samples showing the fossils affected by D_1 and D_2 phases of deformation.
Figura 5. Fotografías de las cinco muestras con braquiópodos deformados por las fases D_1 y D_2.

three fossils were selected with complete hinges and symmetrical lines (figs. 6 and 7).

The results are summarized on a synthetic table (Table 1). A final synthesis will be raised and a conclusion-discussion will be presented as an attempt to identify the significance of this deformation in the genesis of the Variscan chain in a junction zone of five Variscan domains of the western Moroccan Meseta.

4,3. Wellmann method and Breddin graph

The Wellman method (Wellman, 1962; Shah and Srivastava, 2007) uses objects with orthogonal lines of symmetry in the undeformed state, by drawing a reference line and then project on it parallel lines from endpoints to hinge and symmetry lines from each fossil. If the rock is unstrained, the lines will define a rectangle. If the rock is strained they will define parallelograms. At least the numbered corners of the parallelograms are joined to fit an ellipse with major and minor axis, which give the axial ratio *R*. If an ellipse cannot be fitted, then the strain is heterogeneous.

The input data in Breddin graph (Breddin, 1956; Célérier and Séranne, 2001) are the angular shear (ψ) and the orientations of the sheared line pairs with respect to long axis of the strain ellipse (ϕ). The *R*-value or ellipticity of the strain ellipse is found by fitting the points on the plot until they coincide on one of the curves.

Sample	Nº	ψ	γ	2θ'	N_{hinge}	N_{sinus}	Λ_G	Λ_p	Λ_p/Λ'_G	λ_G/λ_P	N λ_G	N λ_P
1	Fossil 1 Fossil 2 Fossil 3	+32º +28º +09º	0,625 0,532 0,758 **γ_m : 0,637**	1-2 : 13º 2/3 : 67º 1/3 : 80º	N009 N022 N030	N145 N136 N163	07	23	3,285	1,813	N167	N77
2	Fossil 1 Fossil 2 Fossil 3	+16º -12º -20º	0,286 -0,212 -0,363 γ_m : -0,289	1-2 : 100º 2-3 : 66º 1-3 : 166º	N001 N137 N088	N113 N025 N002	7,4	16,3	2,202	1,483	N175	N85
3	Fossil 1 Fossil 2 Fossil 3	+06º -25º -21º	0,1051 -0,4663 -0,3838 **γ_m : -0,745**	1-2 : 123º 2-3 : 30º 1-3 : 93º	N041 N111 N170	N175 N019 N042	13,2	33,3	2,523	1,59	N29	N119
4	Fossil 1 Fossil 2 Fossil 3	-8º +25º +10º	-0,1405 0,4663 0,1763 **γ_m : 0,502**	1-2 : 108º 2-3 : 66º 1-3 : 50º	N153 N014 N177	N018 N150 N132	09,2	24,8	2,695	1,641	N162	N72
5	Fossil 1 Fossil 2	-34º -13º	-6,674 -0,231 γ_m : -0,905	1-2 : 70º	N002 N118	N042 N014	7,5	30,6	4,08	2,02	N177	N87

Table 1. Summary of parameters of the distortion of brachiopod fossils of Upper Visean and orientation of the ellipse axes λG, λP. ψ: shear strain; γ= tg ψ; θ': angle between hinges; λ: elongation ; Λ = λ^2 : quadratic elongation ; Λ'p and Λ'_G : reciprocal quadratic elongation as $\Lambda' = \Lambda'_G \cos^2 \theta' + \Lambda'_p \sin^2 \theta'$; λ_G/λ_P : axial ratio of strain ellipse as $\lambda_G/\lambda P = (\Lambda'_p / \Lambda'_G)^{1/2}$; N λ_G and N λ_P : orientation of the ellipse axes.

Tabla 1. Resumen de los parámetros de distorsión de los fósiles de braquiópodos del Viséense Superior y orientación de los eje principales de la elipse λ_G, λ_P. ψ: ángulo de cizalla ; γ= tg ψ: deformación angular ; θ': ángulo entre charnelas de dos fósiles ; λ : elongación ; Λ = λ^2 : elongación cuadrática; Λ'^p y Λ'^G : elongación cuadrática recíproca con $\Lambda' = \Lambda'_G \cos^2 \theta' + \Lambda'_p \sin^2 \theta'$; λ_G/λ_P : relación axial de la elipse $\lambda_G/\lambda_P = (\Lambda'_p / \Lambda'_G)^{1/2}$; N λ_G y N λ_P : Orientación de los ejes principales de la elipse de deformación.

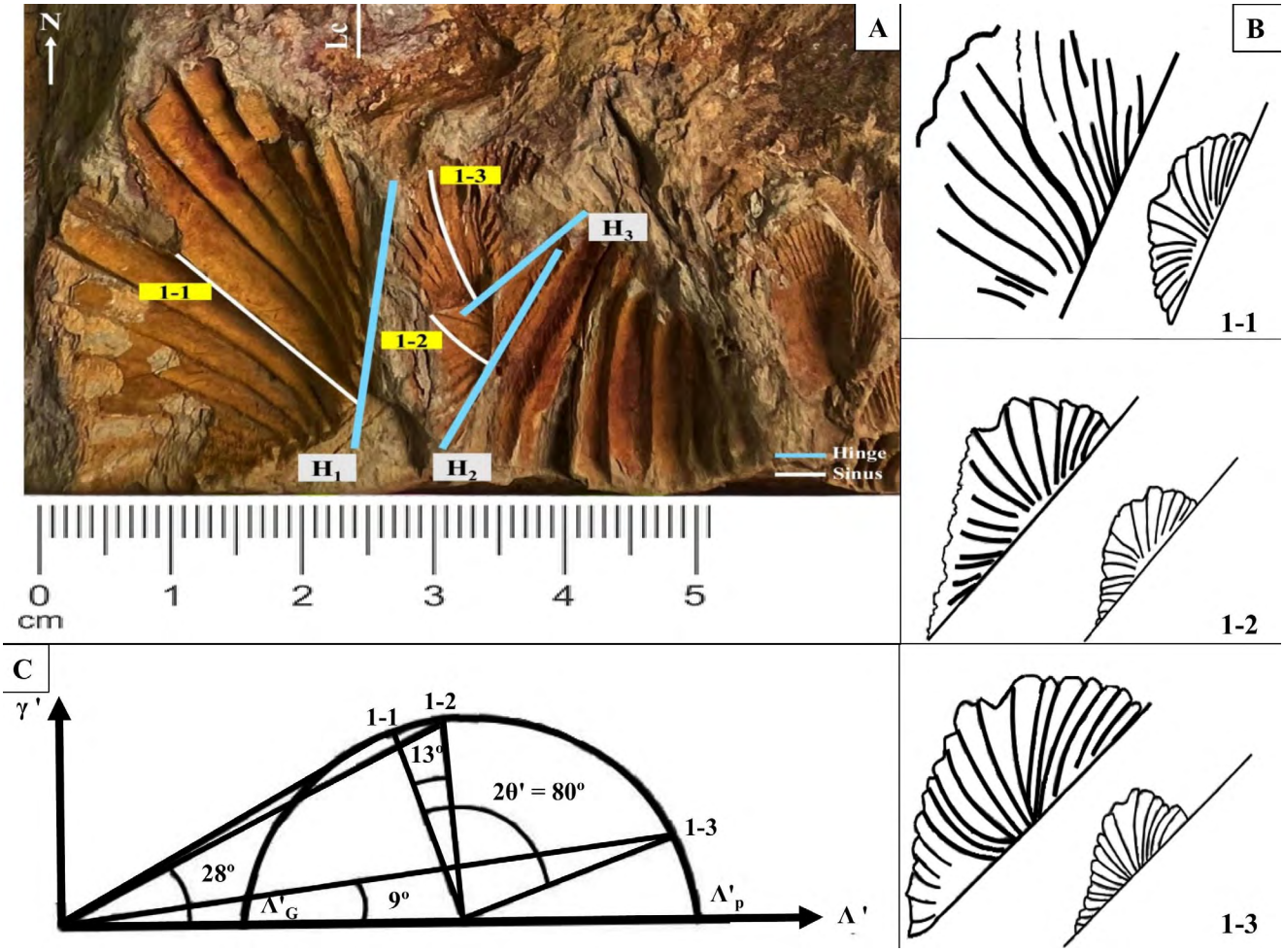

Figure 6. Distortion parameters measured on sample 1. A- Photography of three individuals (H: hinge); B- Aspects of distorted brachiopods 1-1, 1-2, 1-3; C-Mohr diagram of corresponding strain.

Figura 6. Parámetros de distorsión medidos en la muestra 1. A- Fotografía de tres individuos (H: charnela); B- Aspecto de los braquiópodos distorsionados 1-1, 1-2, 1-3; C- Diagrama de Mohr de deformación correspondiente.

5. Results

Sample 1:

This sample taken from the middle of the low-dipping limb of recumbent shows fossils deformed mainly by refolding S_2 P_2 (D2), crenulation especially in the intrados of the minor folds. Among 12 fossils, 3 individuals were selected 1-1, 1-2 and 1-3 (figs. 6-A and B). All the fossils are weakly S-shaped which seems to indicate a heterogeneous deformation. The fossils are commonly micro-folded (N-S trending hinges). The angles 2θ' shown by their hinges are 13°, 67°, and 80°. The construction of the Mohr circle of deformation (Fig. 6-C) considering the parameters (ψ, 2θ'), permit to determine the reciprocal ratio Λ'_P / Λ'_G = 3.2857. The ratio λ_G/λ_P (R) of the ellipse axis we look for is $\lambda_G/\lambda_P = (\Lambda'_P / \Lambda'_G)^{1/2}$ = 1.813.

The trend of λ_G is computed by counting 24° clockwise outside of the angle formed by hinge 1-1 and hinge 1-3, i.e., approximately λ_G is N167°E and λ_P is N077°E. We obtain so the axial ratio and the orientation of the ellipse axis.

Sample 2: (Fig. 7-A)

This sample is the farthest from the hinge of the anticline, and presents great richness in fossils (brachiopods and lamellibranchs). The chosen individuals present two negative ψ values, namely -12° (2-2) and -20° (2-3), and a positive ψ value for 2-1, +16°. Angles 2θ' formed by the three hinges are relatively high (66°, 100°, and 166°). The axial ratio λ_G/λ_P (R) obtained from the Mohr circle is the lowest among all of the studied samples (1.483). The calculated axes of the finite strain ellipse yielded λ_G: N175°E and λ_P: N085°E.

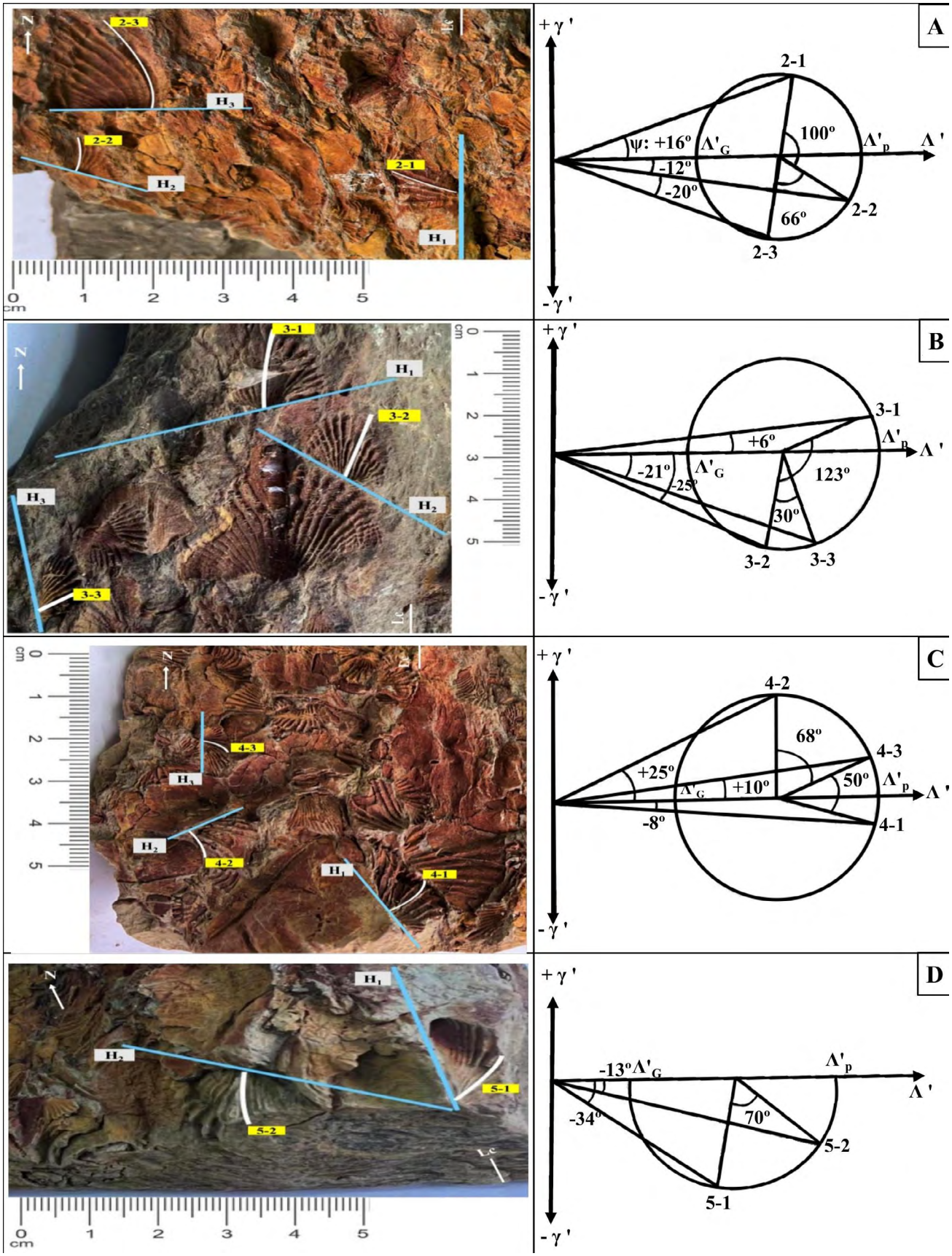

Figure 7. Photographs of chosen shells of samples 2 to 5 (A to D) and Mohr diagram resulting from their angular strain.

Figura 7. Fotografías de braquiópodos escogidos en las muestras 2 a 5 (A a D) y diagramas de Mohr dibujados a partir de su deformación angular.

Sample 3: (Fig. 7-B)

Located at the middle part of the low-dipping limb of the anticline, it shows very big and thin individuals, in average, L (hinge): 3 cm, and l (sinus): 3.5 cm. Most of the shear angle values are negative, -21º (3-3), -25º (3-2) and +6º (3-1). The three hinges are intersected at 123º, 30º and 93º. The axial ratio λ_G/λ_P (*R*) extracted from Mohr circle is 1.59 and the strikes of the ellipse axes are N029ºE (λ_G), and N119ºE (λ_P).

Sample 4: (Fig. 7-C)

This sample is located at a second-order syncline, on the vertical limb of a larger anticline. The three individuals selected cut each other at 2θ' of 108º, 66º and 50º; ψ is mostly positive +10º (4-3), +25º (4-2) and -8º (4-1). The ratio λ_G/λ_P (*R*) obtained is 1.641, and the directions of strain ellipse axes are N162ºE (λ_G), and N072ºE (λ_P).

Sample 5: (Fig. 7-D)

This sample was taken from the hinge of the anticline affected by penetrative crenulation cleavage, which folds intensively the fossils. Only two fossils are complete, 5-1 (ψ = -34º), and 5-2 (ψ = -13º), which hinges cut at 2θ'= 70º. The λ_G/λ_P ratio (*R*) is the highest of all the studied samples, 2.02, and the directions of ellipse axes are N177ºE (λ_G), and N087ºE (λ_P).

From table 1, which summarizes the deformations of the fossil brachiopods of the five samples, we can note the following conclusions:

Positive values of ψ vary between 6º to 32º, while the negative values vary between -12º to -34º.

The λ_G/λ_P ratio (*R*) obtained from the Mohr diagram developed for each fossil group varies between 1.483 and 2.02.

5.1. Strain parameters analysis

5.1.1. Relationship between ψ and 2θ'

The class 60º-80º of the angle 2θ', which is twice the angle between the hinge axis of the brachiopod fossils and the long axis of the finite strain ellipse, is the most representative in terms of variation of the deformation: ψ varies from +9º to +32º clockwise and from -8º to -34º counter-clockwise (Fig. 8). So, it is in the 2θ' class of 60º-80º that we observe a maximum of rotation (+32º and -34º).

5.1.2. Average results

The Mohr circles constructed for the samples show a homogeneous distribution of the shear angle ψ. The distances of the intersections of the circles from the center of the graph (Λ', γ') yield similar values, because the axial ratios λ_G/λ_P (*R*, the root of the ratio Λ'_P/Λ'_G) show values varying only slightly between 1.483 and 2.02 (Table 1). The determination of the mean value of the final axial ratio of the ellipse of deformation in the sampling area, either calculating the average value or directly on the cumulated graph (Λ', γ'), yield the same result: $\lambda_G/\lambda_P = (\Lambda'_P/\Lambda'_G)^{1/2} = 1.7$.

The determination of the orientation of the principal axes of the finite strain ellipse from the Mohr circle gives the following average results (Table 1): $N\lambda_G$ = N170, and $N\lambda_P$ = N082.

5.1.3. λ_G/λ_P ratio and the structural context

The sampling was performed around an N-S-trending, west-vergent anticline (Fig. 1-C). The maximum values of the λ_G/λ_P ratio correspond to the hinge of the fold, on its inner arc, where, assuming a mechanism of tangential longitudinal strain folding, shortening parallel to the layering is the highest (sample 5). Elsewhere from the fold's hinge on the same lumachellic layer the ratio decreases ($\lambda_G/\lambda_P{}^{(1)} = 1.813$ and $\lambda_G/\lambda_P{}^{(4)} = 1.642$), which is also a characteristic of tangential longitudinal strain. These two samples are in symmetrical positions relative to the axial plane around the hinge. On the low-dipping limb, the value decreases to stabilize around 1.5: $\lambda_G/\lambda_P{}^{(3)} = 1.59$ and $\lambda_G/\lambda_P{}^{(2)} = 1.483$.

5.2. Results by using Wellmann method and Breddin graph

Wellman method give a finite strain ellipse fitted by joining corners of the parallelograms. Its long axis is oriented N152 while its short axis is oriented N062. The axial ratio (*R*) is equal to 1.87 (Fig. 9-A).

Input data (ψ, ϕ) of table of Figure 9-B1 are plotted in the Breddin graph, giving *R* values varying between 1.2 and 2.5 (Fig. 9-B2). The axial ratio average is R= 1.7. Note that the average orientations of ellipse axes given by Mohr diagrams are N170 and N082, and λ_G/λ_P or *R*= 1.7.

The results obtained for the ratio R are similar for the three methods (see Table 1 (λ_G/λ_P) and Fig.

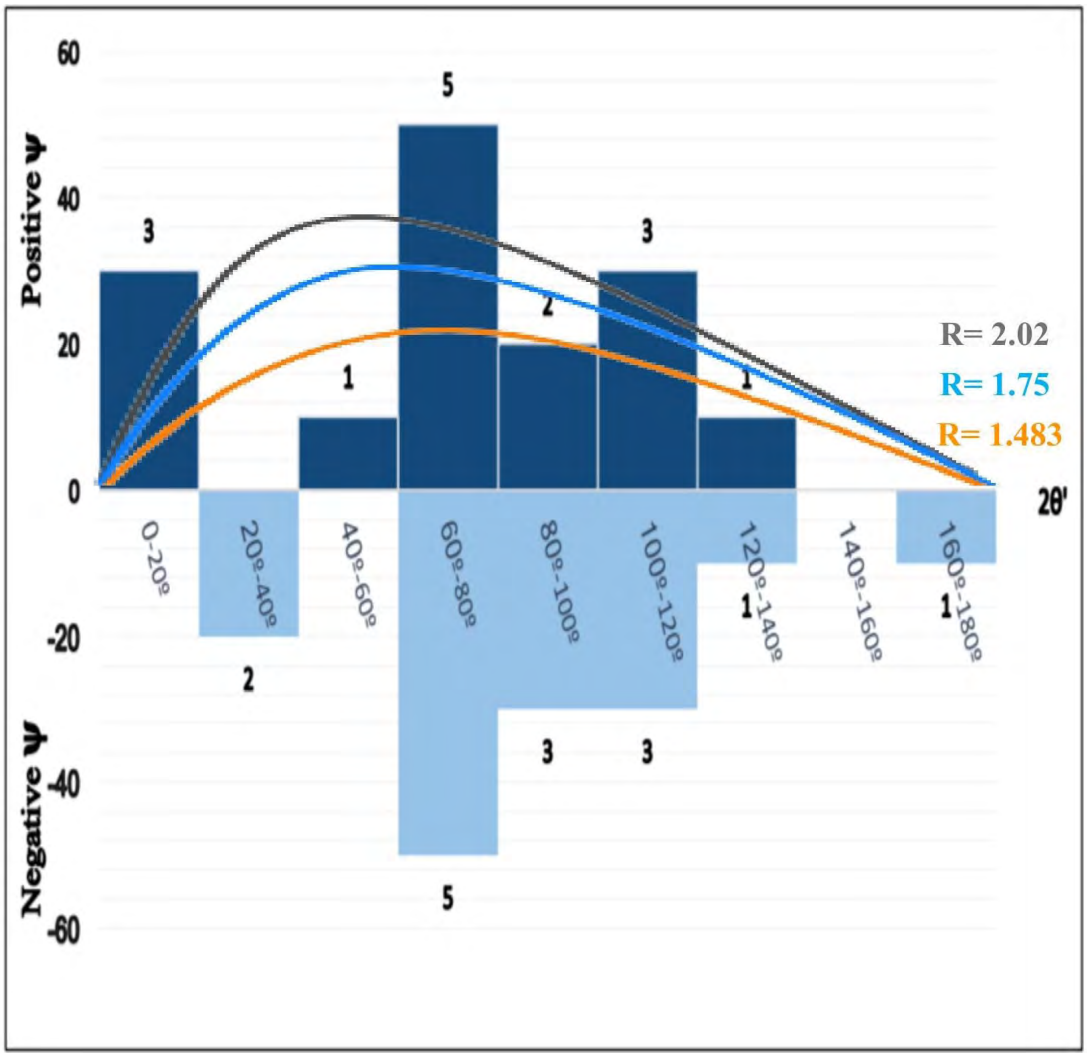

Figure 8. Histogram showing the relationship between the sign of the shear angle ψ and 2θ' angle. The numbers on or below columns indicate the number of fossils (frequency).

Figura 8. Histograma que muestra la relación entre el ángulo de deformación ψ y el ángulo 2θ'. Los números por encima o por debajo de las columnas indican la frecuencia de fósiles.

9): the average values of R=1.697 by Mohr circles, 1.698 by Breddin abacus, and 1.87 by Wellman's method.

6. Conclusion – Discussion

The bulk finite strain computed on strained, Upper Visean brachiopods in the northern area of the Sidi Bettache basin, permits to highlight a possible non-coaxial deformation attained by the brachiopod shells (Fig. 10). Strain was generated under E-W shortening, as a progressive deformation during folding and the development of crenulation cleavage (D_2). The three methods used to determine the strain ellipse (Mohr, Wellmann and Breddin) yielded the same results: long and short axes of the finite strain ellipses: N152 to N170 and N62 to N82, respectively, while the average *R* value is of 1.7 (Mohr and Breddin) or 1.87 (Wellmann).

Deformation is partially computed and described by its strain parameters (ψ, γ, λ_G/λ_P) on deformed brachiopods. Distortion of shells took place probably within N-S trending shear zones formed under ductile dextral transpression (Fig. 10-B). These structures were recently recognized (Nassri and El Adraoui, 2022; Nassri *et al.*, 2023) in the neighboring domain (Benslimane basin) in which the Famennian-Visean series are exposed over a relatively large surface.

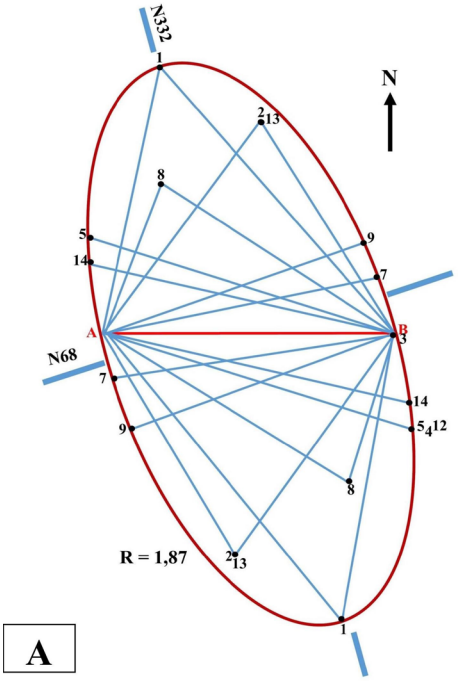

Sample	ψ	Φ	R
1 (1-1)	+32º	+18º	2
2 (1-2)	+28º	+50º	2
3 (1-3)	+09º	+13º	1,3
4 (2-1)	+16º	+07º	2
5 (2-2)	-12º	-26º	1,3
6 (2-3)	-20º	-60º	1,7
7 (3-1)	+06º	+80º	1,5
8 (3-2)	-25º	-30º	1,6
9 (3-3)	-21º	-19º	1,6
10 (4-1)	-08º	-07º	1,4
11 (4-2)	+25º	+60º	2,5
12 (4-3)	+10º	+10º	1,4
13 (5-1)	-34º	-20º	2
14 (5-2)	-13º	-64º	1,5

B1

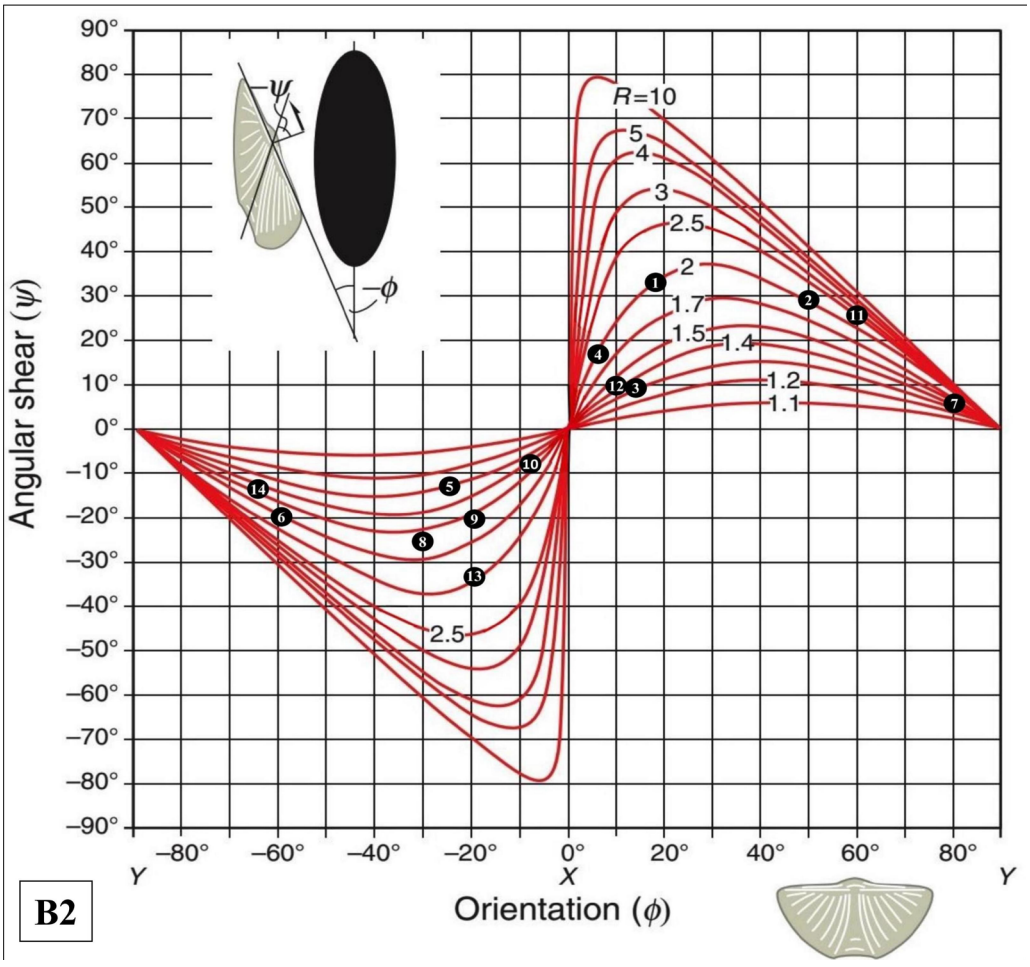

Figure. 9. A-Ellipse orientations and R-value obtained by Wellman method; B1- Table (ψ, Φ, R) summarizing data and results by Breddin abacus (B2).

Figura. 9. A-Orientaciones de elipses y valor de R obtenidos por el método de Wellman; B1- Tabla (ψ, Φ, R) que resume los datos y resultados por el ábado de Breddin (B2).

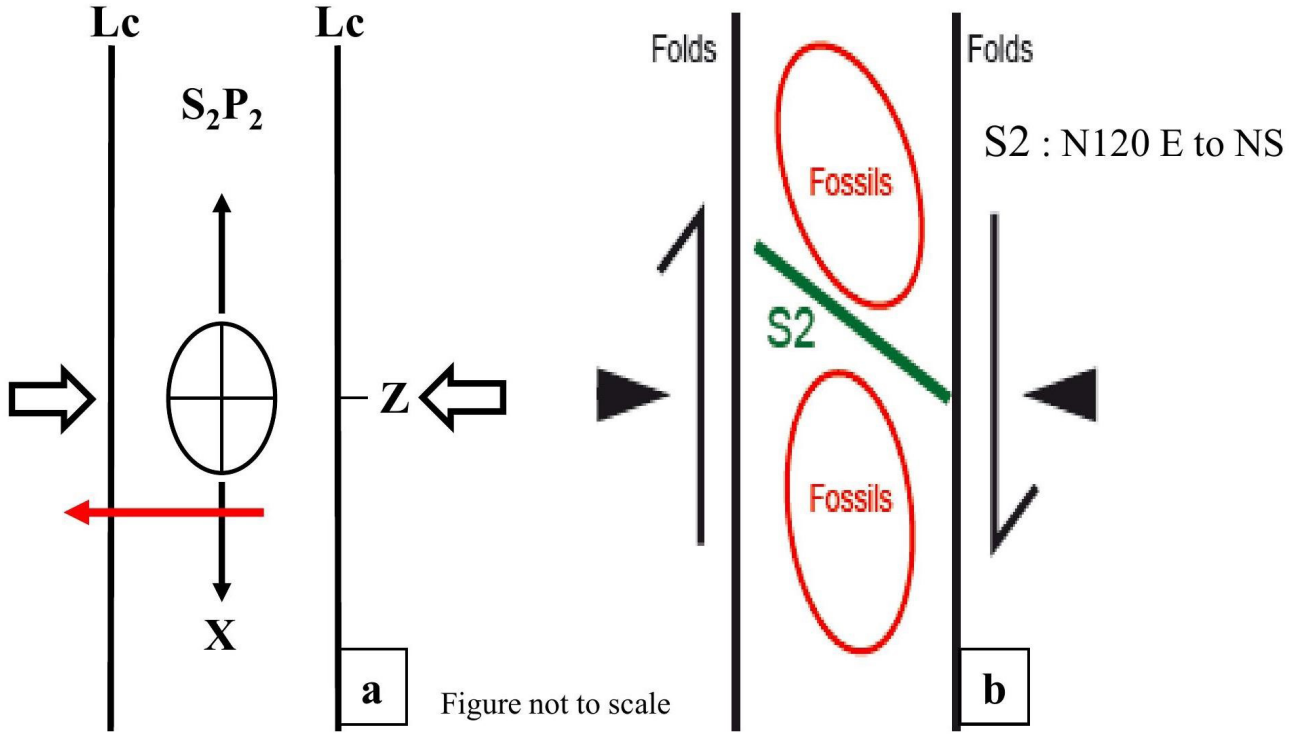

Figure 10. Main stages of dextral transpression D_2 (EW shortening) in the northern part of the Sidi Bettache Basin: a-Folding and crenulation cleavage; b-Distortion due to NS simple shear; Red arrow: Sense of matter transfer.

Figura 10. Etapas principales de transpresión dextra D_2 (acortamiento EO) en la parte norte de la cuenca de Sidi Bettache: a-Plegamiento y esquistosidad de crenulación; b-Distorsión por cizalla simple N-S; Flecha roja: Sentido transferencia de la materia.

In the studied area, it is important to note the absence of semi-brittle tectonics by pressure-solution in shales, and lumachellic muds and dark clays show plastic behavior. According to Vialon (1991) isotropic layers must be subjected to a strong average stress (σ_1-σ_3). Indeed, clays contain water which, if it is not expelled during shortening, can make the process reversible or result in superimposed cleavages (Gratier, 1984; Vialon, 1979). The appearance of schist anisotropy corresponds to a preferential orientation of the internal matter by continuous ductile deformation. In presence of fluids, two behaviors can occur during the generation of schists (Nicolas and Vialon, 1980; Gratier, 1984):

- Reorientation by rotation of the objects (crystals, grains, shells) is synchronous with the loss of water, which leads to compaction and hardening of the clay.
- Pressure-solution cleavage (Rutter, 1983): in this case the shortening of grains parallel to the major stress axis gives changes in form and volume.

The deformations observed on the Upper Visean brachiopod schists correspond to the first case.

The studied area lies a few tens of meters from the N-S shear zone that separates Cherrat Ridge to the west from Sidi Bettache basin to the east (Fig. 1-B). This shear zone acted as a dextral ductile shear band, such as is the case for the Bouznika shear zone (Laamrani, 1993; El Attari, 2021).

In the northern part of Sidi Bettache basin, the pure ductile behavior of Carboniferous series can be explained by the proximity of the N-S Cherrat band, which contributed to the displacement to the north of the western Meseta. This type of struc-

tures is common elsewhere throughout the Variscan Orogen, such as in the neighboring Iberian Massif (Díez Fernández and Martínez Catalán, 2012; Díez Fernández and Pereira, 2017), where they also occur alongside sinistral strike-slip shear zones during the latest stages of Variscan deformation (Díez Fernández *et al*., 2021). These structures are responsible for the displacement of previously deformed pieces of the Variscan Orogen, usually juxtaposing rock series with contrasting tectonothermal evolution and provenance.

References

Ait Brahim, L., and Tahiri, A. (1996). Rotation horaire des contraintes et mécanismes d'ouverture et de fermeture des bassins permiens du Maroc central. In: F. Medina (ed.): Le Permien et le Trias du Maroc, état des connaissances. Edit. Pumag, Marrakech, pp. 87-98.

Breddin, H. (1956). Die tektonische Deformation der Fossilien im Rheinischen Schiefergebirge. Zeitschrift Deutsche Geologische Gesellschaft, 106, 227-305.

Chalouan, A. (1977). Stratigraphie et structure du Paléozoïque de l'Oued Cherrat : un segment du couloir de cisaillement de la Meseta Occidentale, Maroc. Thèse de 3éme cycle, U.L.P. Strasbourg, 92 p.

Célérier, B., and Séranne, M. (2001). Breddin's graph for tectonic regimes. Journal of Structural Geology, 23, 789-801.

Destombes, J., and Jeanette, A. (1966). Mémoire explicatif de la carte géotechnique de la Meseta côtière à l'Est de Casablanca au 1/50000. Région de Mohammedia, Bouznika, Ben-Slimane. Notes et Mém. Serv. géol. Maroc, 180 bis, 104 p.

Díez Fernández, R., Fernández, C., Arenas, R., and Novo-Fernández, I. (2021). On the Rootless Nature of a Devonian Suture in SW Iberia (Ossa-Morena Complex, Variscan Orogen): Geometry and Kinematics of the Azuaga Fault. Tectonics, 40(6), e2021TC006791. https://doi.org/10.1029/2021TC006791.

Díez Fernández, R., and Martínez Catalán, J. R. (2012). Stretching lineations in high-pressure belts: the fingerprint of subduction and subsequent events (Malpica–Tui complex, NW Iberia). Journal of the Geological Society, 169, 531-543. https://doi.org/10.1144/0016-76492011-101.

Díez Fernández, R., and Pereira, M. F. (2017). Strike-slip shear zones of the Iberian Massif: are they coeval? Lithosphere, 9(5), 726-744. https://doi.org/10.1130/L648.1.

El Attari, A. (2021). Etude lithostratigraphique et tectonique des terrains paléozoiques du môle côtiér (meseta occidentale, Maroc). Thése de Doctorat. Universite Mohammed V-Agdal. Faculté des Sciences de Rabat.

El Hadi, H., Tahiri, A., Cabrera, F. *et al*. (2006). Un exemple de volcanisme calco-alcalin de type orogénique mis en place en contexte de rifting (Cambrien de l'oued Rhebar, Meseta occidentale, Maroc). Comptes Rendus Geoscience, 338, 229-236.

Fossen, H. (2010). Structural Geology. Cambridge University Press, 1-463. https://doi.org/10.1017/CBO9780511777806.

Gratier, J. P. (1984). La déformation des roches par dissolution-cristallisation: aspects naturels et expérimentaux. Thèse de, Univ. Grenoble.

Laamrani El Idrissi, A. (1993). Relations déformations-Déplacements le long des failles hercyniennes : système de Bouznika et système de Cherrat-Benslimane et du Cherrat-Ykem. th Des de 3e cycle, Univ. Med V.,Fac,sc.,Rabat, 213 p.

Lakhloufi, A., Hamoumi, N., Saquaque, A., *et al*. (2002). Évolution géodynamique des bassins de Sidi Bettache et de Brachwa-Maaziz et reinterpretation de l'histoire de l'Orogénese Hercynienne post-Viséenne au Maroc. 519 págs. Thèse Sciences Université Mohammed V., Rabat.

Lakhloufi, A., Hamoumi, N., Saquaque, A., *et al*. (2008). Tectónica compresiva sinsedimentaria de edad Viseense Superior en la cuenca de Sidi Bettache (Meseta noroccidental marroquí) Late Visean synsedimentary compressive tectonism into the Sidi Bettache Basin (northwestern Moroccan Meseta). Bol. R. Soc. Esp. Hist. Nat. Sec. Geol., 102(1-4), 71-92.

Lecointre, G. (1926). Recherches géologiques dans la Meseta marocaine. Mém. Soc. Sci. natur. Maroc, 14, 158 p.

Michard, A. (1976). Elément de la géologie du Maroc. Notes et Mémoires du Service géologique du Maroc, 252, 422 p.

Michard, A. (1977). Contraintes, déformations, fabriques-ULP,institut de Géologie-strasbourg 150 p.

Nassri, K., and El Adraoui, A. (2022). Rôle Des Alternances De Tectoniques Ductile Semi Fragile – Fragile Avec Σ1 Decrescendo En Rotation Horaire, Dans La Structuration Hercynienne De La Façade Nord De La Bande De Benslimane (Meseta Nw, Maroc). The International Congress on Educational Research, Materials Science & Engineering (ICEMSE) Saidia, Marocco, 25-27 November 2022, 71p. http://icsse2022.com/wp-content/uploads/2022/11/Proceeding.pdf.

Nassri, K., El Adraoui, A., and Tahiri, A. (2023). Etude microtectonique des déformations synsédimentaires des terrains dévono-carbonifères de la plage de Skhirate (Nord de la bande de Benslimane, Meseta NO, Maroc). Hypothèse d'un bassin pull-apart en relai sur la branche Nord de la zone de cisaillement dextre de la Meseta occidentale (ZCMO). Bulletin

de l'Institut Scientifique, Rabat, Section Sciences de la Terre, 2023, n° 45, 61-81.

Nicolas, A., and Vialon, P. (1980). Les mécanismes de déformation ductile dans les roches. Livre Jubil. 1830-1980, Mém. H. s. Soc. Géol. France, 10, 127-139.

Nicolas, A. (1984). Pricipes de Tectonique, Ed. Masson, Paris, 196 p.

Piqué, A. (1979). Evolution structurale d'un segment de la chaîne hercynienne : la Meseta marocaine nord-occidentale. Sci. Géol., Mém. 56, 243p.

Piqué, A. (1994). Géologie du Maroc : les domaines régionaux et leur évolution structurale. Ed. Pumag. 239 p.

Piqué, A., Soulaimani, A., Hoepffner, C., *et al.* (2006). Géologie du Maroc Editions GEODE, Marrakec, 271 p.

Ramsay, J. G. (1967). Folding and fracturing of rocks. McGraw-Hill, New-York. 568 p.

Ramsay, J. G., and Graham, R. H. (1970). Strain variation in shear belts. Canadian Journal of Earth Sciences, 7(3), 786-813.

Rutter, E. H. (1983). Pressure-solution in nature, Theory and experiment. J. Geol. Soc. London, 140, 725-740.

Shah., J., and Srivastava, D. C. (2007). Strain estimation from distorted vertebrate fossils: application of the wellman method. Geology Magazine, 144(1), 211-216.

Vialon, P. (1979). Les déformations continues-discontinues des roches anisotropes. Eclog. Helveticae, 79(2), 531-549.

Vialon, P. (1991). Objet et démarche de la tectonophysique. Revue Française de géotechnique, Nº 56, 7-15.

Wellman, H. G. (1962). A graphic method for analyzing fossil distortion caused by tectonic deformation. Geological Magazine, 99, 348-52.